Fibers of aligned single-walled carbon nanotubes: Polarized Raman spectroscopy

H. H. Gommans,[a] J. W. Alldredge,[b] H. Tashiro, J. Park, J. Magnuson,[c] and A. G. Rinzler[d]
Department of Physics, University of Florida, Gainesville, Florida 32611

(Received 14 March 2000; accepted for publication 19 May 2000)

To probe the one-dimensional nature of single-wall carbon nanotubes (SWNTs) in bulk samples, we have devised a simple method for generating fibers of aligned SWNTs. We measured polarization-dependent Raman spectra on the oriented fibers. Contrary to what is expected from their theoretically assigned vibration-mode symmetries, *all* the Raman line intensities are observed to decrease in nearly *equal* amounts for the 647.1 nm laser excitation polarized perpendicular to the fiber axis versus that polarized parallel to the fiber axis. The effect is explained as a loss of resonance Raman scattering for the perpendicular polarization case. © *2000 American Institute of Physics.* [S0021-8979(00)00517-X]

I. INTRODUCTION

Low-dimensional systems provide a fruitful area of research both for the properties that can arise from the reduced dimension and for elucidation of emergent properties in three dimensions. Single-walled carbon nanotubes (SWNTs), with their well-defined atomic structure, chemical stability, small diameters, and high aspect ratios, constitute wonderful one-dimensional (1D) molecules for investigating 1D effects. An important recent example is provided by the sharp Van Hove singularities observed in tunneling spectroscopy measurements on individual nanotubes.[1,2]

In present high-yield methods of synthesis, the nanotubes self-assemble into well-ordered bundles of a few to several hundred aligned tubes ("ropes").[3,4] These ropes, however, are highly entangled with each other, resulting in a highly disordered bulk material. The anisotropy of the individual nanotubes expected from their 1D character becomes orientationally averaged, reducing the information that might be obtained by macroscopic probes. To address this issue, we have developed a simple method for generating bulk fibers of SWNTs possessing substantial alignment of the nanotubes along the fiber axis. Other reports have appeared in the literature claiming alignment of SWNTs; however, few measurements demonstrating a sample anisotropy have been reported.

As a first investigation with these aligned SWNTs, we undertook to verify the vibrational-mode assignments of Raman spectral peaks which have appeared in the literature.[5,6] The relative intensities of Raman lines recorded with the exciting light polarized parallel in one measurement and perpendicular in another to the relevant crystallographic axis of an oriented sample can often provide conclusive identification of the symmetry species of the vibrational mode responsible for the line. Because oriented nanotube samples have not previously been available, all assignments have been based strictly on modeling. As we describe below, the 1D character of the nanotubes complicates the application of polarized Raman measurements for making such mode assignments.

II. EXPERIMENTAL DETAILS

The aligned SWNT fibers were assembled from highly purified,[7] laser-vaporization-grown[3] SWNTs dispersed by ultrasonication in *N*,*N*-dimethylformamide (DMF). SWNT concentrations of ~0.01 mg/ml were used. Generation of a SWNT fiber proceeds as follows. A commercially available carbon fiber (unsized, highly graphitized, 8 μm diam), approximately 12 mm long, is first attached to one end of a 10-mm-long, 0.5-mm-diam wire, with conductive silver paint. The wire is supported in a pin vice, which is itself attached to a motor-driven translation stage. This permits the carbon fiber (CF) to be translated down along its axis into the SWNT suspension, to a depth of about 8 mm (Fig. 1). The pin vice is electrically isolated from the stage such that a voltage can be applied between the CF and a platinum wire that is also submersed in the SWNT/DMF suspension. At voltages of 1–2 V, with the CF the positive electrode, a cylindrically symmetric cloud of the SWNT is observed to form around the CF over the course of several minutes. Upon formation of this cloud (10–30 min) the CF is slowly withdrawn from the suspension, with the motor providing a smooth, steady rate of retraction. As the CF pulls out of the liquid it is seen to have attached to its end another fiber that forms spontaneously from the assembled cloud of nanotubes. The length of the assembled fiber is limited mainly by the travel range of the translation stage, the size of the SWNT cloud formed, and the smoothness of the withdrawal.

Generation of the SWNT fiber can be likened in this process to the withdrawal of highly entangled seaweed from the surface of the sea. The mass remaining below the surface,

[a]International exchange student; permanent address: University of Utrecht, Utrecht, The Netherlands.
[b]University of Florida Undergraduate Scholars Program.
[c]NSF-UFL Summer Research for Undergraduates Program; permanent address: Department of Physics, Yale University, New Haven, CT.
[d]Author to whom correspondence should be addressed.

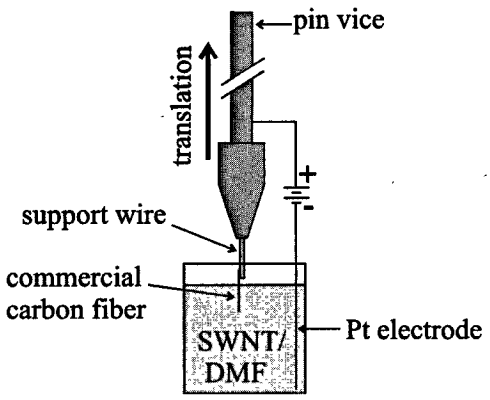

FIG. 1. Aligned SWNT fiber production setup. A potential of 1–2 V is applied between the commercial carbon fiber and the platinum counterelectrode for 10–30 min, assembling the interconnected SWNT cloud. When the commercial fiber is slowly withdrawn from the solution it "draws" the aligned SWNT fiber.

and the surface tension, act to generate a vertical stress field which works to align the strands vertically. The surface tension in the fluid meniscus, where the strands exit the surface, acts to pull these strands together into a single cohesive bundle. Analogy may also be made with the melt-spinning process for producing polymer fibers (e.g., nylon 6), which similarly results in molecular alignment along the fiber axis.

The formation of the SWNT cloud about the positively charged CF indicates that the nanotubes, like other polycyclic aromatic carbon structures, pick up negative charge from their environment and migrate electrophoretically to the positive electrode. The highly polar DMF does not permit the field to penetrate very deeply into the suspension, however, so the aggregation of the SWNT is likely a diffusion-limited process. Formation of the visible cloud occurs on the relatively slow time scale of minutes. A steep concentration dependence of the time taken to form comparably dense SWNT clouds similarly suggests a diffusion-limited cloud assembly.

The mechanism by which DMF yields a metastable suspension of the SWNT remains to be determined. The evidence in this work suggests that the suspension is charge stabilized by the same negative charge affording the nanotubes their electrophoretic mobility. Once this excess charge is removed by oxidation at the positive electrode, the nanotubes lose their charge-generated repulsive stabilization. With their lyophobic surfaces now in contact, the nanotubes stick to the (graphitic) electrode, and to each other, forming the cohesive mass surrounding the electrode. Once they have touched, and are charged to the same positive potential, the free ends of the nanotubes would repel each other, preventing the assembled structure from collapsing on itself. The microscopic structure of the cloud is likely highly dendritic with an extremely large number of branches.

We have produced dozens of SWNT fibers by this method. The fiber diameters are, typically, 2–10 μm depending on the time allowed for the SWNT cloud assembly before withdrawal, and the rate of withdrawal. As mentioned above, the length of the fibers is limited mainly by the travel range of the translation stage. A recently added long-travel

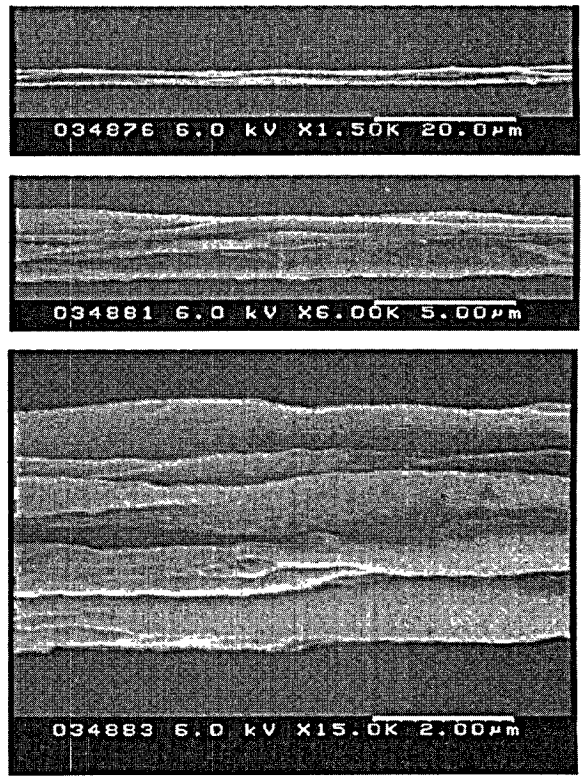

FIG. 2. Scanning electron micrographs of an aligned SWNT fiber recorded at three different magnifications (magnifications indicated by corresponding scale bars).

stage has generated fibers up to 5 cm in length. Given a method for replacing the SWNT lost from the solution to the fiber, there is no reason, in principle, why the process could not be made to work continuously, producing aligned SWNT fibers of arbitrary lengths.

We have imaged SWNT fibers made in this manner by scanning electron microscopy (SEM), high-resolution transmission electron microscopy (TEM), and performed selected area electron diffraction (SAED). The latter two probes are restricted to the sides of the fibers, where the cross section is thin enough to allow transmission of the electron beam. Consistent with alignment of the SWNT along the fiber, the SAED shows two small, somewhat diffuse, spots aligned on either side of the direct beam spot oriented at 90° to the fiber axis. The angular extent of the spots suggests that the bulk of the ropes lie within ~25° of the fiber axis. This is confirmed by direct TEM imaging of the rope lattice, which apart from some occasional gross misalignment, shows the ropes to lie largely along the fiber axis. SEM images of a typical fiber made by this process are shown in Fig. 2.

Polarized Raman spectra of the fibers were recorded in the backscatter geometry with a micro-Raman spectrometer (Renishaw Ramanscope 1000) fitted with a 50× 0.65 numerical aperture objective. Excitation was provided by the 647.1 nm line of a polarized krypton ion laser. Total power to the sample was filtered down to 100 μW over the roughly 1–2 μm laser spot. To prevent their vibration, the nanotube fibers were adhered to a polished silicon wafer surface by a drop of methanol. A motorized $x-y$ stage and a rotational stage were used to rotate the fiber angle with respect to the

electric vector of the linearly polarized excitation. Local landmarks were employed to ensure that the same segment of the fiber was being sampled in measurements rotated with respect to each other. Nevertheless, to ensure that the Raman intensity ratios from the measurements were not being skewed by local variations in the degree of SWNT alignment, several measurements were recorded for each general location after slight repositioning.

The transmission of light through a spectrometer can be notoriously polarization sensitive. For polarization-dependent studies, the Renishaw instrument avoids this problem by restricting the light reaching the entrance slit to one particular polarization axis. To accommodated polarization measurements rotated by 90° with respect to this axis, a half-wave plate is inserted just ahead of the polarizer, which rotates the input polarization to the latter by 90°. To ensure that our intensities were not being skewed by other instrumental effects, we checked the transmitted intensity of unpolarized white light over the spectral range of our measurements both with, and without, the half-wave plate inserted. The intensities differed over the entire spectral range by less than 1.5%.

III. RESULTS

Interpretation of Raman scattering spectra from the SWNT was first provided in a seminal paper by Rao *et al.*[5] Based on theoretical calculations, Raman spectra recorded with a range of laser excitations, and tightly reasoned arguments, they were able to show that Raman scattering from the SWNT is a resonantly enhanced process; the resonance occurring with optical transitions between Van Hove singularities in the 1D density of states of the nanotubes. The Raman peaks discussed below correspond, for our sample, to what has been assigned as a radial A_{1g}, tube breathing mode at ~202 cm^{-1} (for 647.1 nm excitation) while the lines near 1590 cm^{-1} are assigned to tangential A_{1g}, E_{1g}, and E_{2g} modes.[5,8]

Saito *et al.*[8] have calculated the polarization and sample orientation dependence of the Raman intensity for a (10,10) SWNT within the nonresonant bond-polarization theory. This model predicts significant differences in the *relative* intensities of the radial and the tangential modes for polarization parallel versus perpendicular to the nanotube axis. The spectra shown in Fig. 3 were recorded on an aligned SWNT fiber at several angles between the incident polarization and the fiber axis ranging from 0° to 90°. For direct comparison to the theoretical intensity predictions, the spectra were recorded with an analyzer having its polarization axis parallel to the incident polarization (*VV* geometry). Apart from subtle differences in the spectra, the dominant effect is a dramatic *overall* loss of intensity in *all* lines for the perpendicular excitation with no change evident in the relative intensities of the radial and the tangential modes.

IV. DISCUSSION

This discrepancy between theory and observation begs explanation, which we now attempt to provide. Since the Raman spectra of the SWNT are resonantly enhanced, consideration of what would make all Raman lines (independent

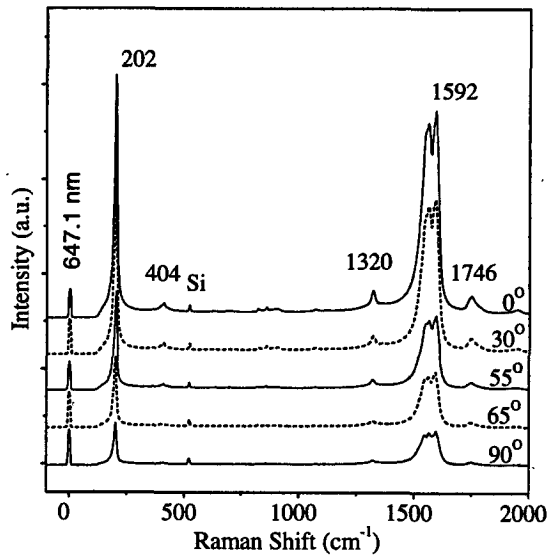

FIG. 3. Raman spectra of an aligned SWNT fiber with the fiber axis at 0°, 30°, 55°, 65° and 90° with respect to the excitation polarization direction. Spectra have been offset for clarity. Excitation is provided by the 647.1 nm line of a krypton ion laser. The analyzer polarization direction is parallel to the incident polarization (*VV* sampling geometry). The line appearing at ~520 cm^{-1} is the Si substrate on which the fiber is placed. Wave numbers of the principle lines are labeled. Note that the intensity decreases proportionately in all lines with increasing angle. Charge transfer from acids intercalated during the purification process results in slightly higher vibration frequencies than in the raw SWNT (see Ref. 7).

of their symmetry species) vanish with the polarization angle suggests the idea of an angle-dependent resonance enhancement. Since resonance Raman arises from resonant absorption, this suggests, in turn, an angle-dependent optical absorption for the nanotubes. In fact, it would be surprising if the 1D character of the nanotubes did not manifest itself as an anisotropy in their spectral absorption cross section. Such an effect was predicted by Ajiki and Ando[9] who, based on $\mathbf{k}\cdot\mathbf{p}$ theory and a depolarizing field occurring for light polarized perpendicular to the nanotube axis, conclude that "interband optical transitions among valence and conduction bands near the Fermi level can be observable only for polarization parallel to the tube axis."

This is confirmed by reflectivity measurements performed on our aligned fibers.[10] For the excitation polarized parallel to the fiber axis, we observe a reflectance peak centered at ~653 nm (84 nm full width at half maximum), which corresponds to the interband optical transitions expected for the metallic nanotubes in the sample (~1.9 eV). With the excitation polarized perpendicular to the fiber axis, however, the reflectivity in this region is flat, indicating the absence of these interband transitions for this polarization.

The resonant absorption for 1.92 eV excitation thus displays an orientation dependence that scales with the direction cosine between the nanotube axis and the incident light polarization direction. This directional dependence can be represented quite simply via the polarizability tensor. For a nanotube oriented along the z axis, the 3×3 polarizability tensor would have components (normalized to 1) $\alpha_{zz}\cong 1$ with all other components $\alpha_{ij}\cong 0$. This yields a dipole moment vector $\mathbf{M}=\underline{\alpha}\cdot\mathbf{E}$ directed along the nanotube axis that

scales with the projection of **E** onto the z axis (along which the nanotube is oriented). The absorption intensity, which goes like $|\mathbf{M}|^2$ will thus depend upon $\cos^2\phi$, where ϕ is the angle between **z** and **E**.

The Raman scattering intensity depends on the squared derivative of the polarizability with respect to each vibrational normal-mode coordinate q_i, i.e., $|d\underline{\alpha}/dq_i|^2$. For the case of nonresonant Raman scattering, the symmetry of this "derived polarizability tensor" is generally quite different from that of the polarizability $\underline{\alpha}$, reflecting rather the normal-mode symmetry through its modulation of the polarizability tensor components with the change in the q_i during the vibration. This situation can change dramatically in the case of resonant scattering.

To demonstrate this, we consider a simple Lorentz oscillator model,[11,12] which displays the salient features. Here, the frequency-dependent electronic polarizability tensor is given by

$$\underline{\alpha}=\sum_j \frac{\frac{e^2}{m}\cdot\underline{\mathbf{F}}_j}{\omega^2-\omega_{oj}^2-i\omega\gamma}, \tag{1}$$

where e and m are, respectively, the electronic charge and mass, ω is the incident radiation frequency, ω_{oj} is the frequency of the jth allowed electronic transition, γ a damping coefficient, and $\underline{\mathbf{F}}_j$ are the oscillator strengths for the transitions. Note that the latter are tensors which contain the orientation dependence appearing in the polarizability. Far from a resonance, the dipole moment given by the last expression enters into the Rayleigh scattering from the molecule. On resonance, this gives the electric dipole transition moment describing resonant absorption.

To make the connection to Raman scattering, we take the derivative with respect to the normal coordinate q (we consider only a single normal mode),

$$\frac{d\underline{\alpha}}{dq}=\sum_j\left[\frac{2\omega_{oj}\frac{e^2}{m}\underline{\mathbf{F}}_j}{(\omega^2-\omega_{oj}^2-i\omega\gamma)^2}\frac{d\omega_{oj}}{dq}+\frac{\frac{e^2}{m}}{\omega^2-\omega_{oj}^2-i\omega\gamma}\frac{d\underline{\mathbf{F}}_j}{dq}\right]. \tag{2}$$

Away from resonance, the first term falls off rapidly leaving only the second term which describes normal, nonresonant Raman scattering. Near a resonance both terms are resonantly enhanced, however, the first term dominates through its more rapidly vanishing denominator. We note that this term acquires its orientation dependence from the $\underline{\mathbf{F}}_j$ tensor and moreover that *this orientation dependence is the same as that of the polarizability itself* (modulated within this envelope by $d\omega_{oj}/dq$).

Since, as indicated above, the polarizability for the 1.92 eV excitation is such that the absorption intensity $I_A\propto|\underline{\alpha}\cdot\mathbf{E}|^2\propto\cos^2\phi$, if the resonance Raman scattering is dominated by a form of the first term above, we anticipate the same angular dependence in the Raman intensity.

The intensity for resonant Raman scattering is typically some tens to thousands of times greater than that for nonresonant Raman scattering. If the foregoing arguments are correct, we expect a dramatic decrease in the Raman intensity for nanotubes oriented perpendicular to the excitation polarization. For our aligned nanotube fibers, while the Raman signal *is* significantly decreased in this configuration, it is only smaller by a factor of ~5. We must, however, consider the effect of nanotubes misaligned from the fiber axis. To explore the effect of these we have considered the following model for comparison to experiment. The measurements include a polarization analyzer so that the measured Raman intensity is given by

$$I_R\propto\left|\mathbf{e}_s\cdot\frac{d\underline{\alpha}}{dq}\cdot\mathbf{e}_L\right|^2\propto|\mathbf{e}_s\cdot\underline{\alpha}\cdot\mathbf{e}_L|^2, \tag{3}$$

where $\mathbf{e}_L$ and $\mathbf{e}_s$ are the unit polarization vectors of the incident and analyzed polarizations, respectively. The second proportionality assumes that a form of the first term in Eq. (2) dominates the Raman scattering completely. We define our experimental geometry as follows, the excitation propagates along **x** with polarization along **z** such that $\mathbf{e}_L=(0\,0\,1)$. The Raman signal is backscattered along **x**, with the analyzer set at either $\mathbf{e}_{s\parallel}=(0\,0\,1)$ (parallel to $\mathbf{e}_L$) or $\mathbf{e}_{s\perp}=(0\,1\,0)$ (perpendicular to $\mathbf{e}_L$). For the nanotube along **z** we take $\underline{\alpha}_z$ as given by $\alpha_{zz}=1$, with all other $\alpha_{ij}=0$. For other angles in the yz plane we have $\underline{\alpha}=\underline{\mathbf{R}}^T\cdot\underline{\alpha}_z\cdot\underline{\mathbf{R}}$ where $\underline{\mathbf{R}}$ is the matrix for rotations about **x**. With these definitions, the last expression gives for the nanotube-angle-dependent scattering intensity for the analyzer parallel

$$VV(\phi)=I_R(e_{s\parallel},\phi)\propto\cos^4\phi, \tag{4}$$

and for the analyzer perpendicular

$$VH(\phi)=I_R(e_{s\perp},\phi)\propto(\cos^2\phi)(\sin^2\phi), \tag{5}$$

where $VV(\phi)$ (analyzer parallel to excitation polarization) and $VH(\phi)$ (analyzer perpendicular to laser polarization) merely simplify the notation. For a measurement with our fiber oriented at an angle ψ with respect to the z axis (in the yz plane), we can account for the Raman intensity contribution of misaligned nanotubes by integrating over angles about ψ. In particular, we consider a model in which a mole fraction of tubes in our fiber p are uniformly distributed within an angle θ about the fiber axis, while the rest $(1-p)$ are uniformly distributed over the other angles $(\pi-\theta)$. Thus, for example, for a measurement with the fiber axis along z ($\psi=0$), we anticipate a Raman intensity

$$VV(0)\propto p\int_{0-\theta}^{0+\theta}VV(\phi)d\phi+(1-p)\int_{\theta}^{\pi-\theta}VV(\phi)d\phi, \tag{6}$$

while for the same incident and analyzed polarizations but with the fiber aligned now at $\psi=\pi/2$,

$$VV(\pi/2)\propto p\int_{\pi/2-\theta}^{\pi/2+\theta}VV(\phi)d\phi+(1-p)\times\left[\int_0^{\pi/2-\theta}VV(\phi)d\phi+\int_{\pi/2+\theta}^{\pi}VV(\phi)d\phi\right]. \tag{7}$$

The ratio $VV(0)/VV(\pi/2)$ (with adjustable parameters p and θ) can now be compared to the ratio of Raman peak

TABLE I. Peak Raman intensities and their ratios for the polarization-analyzer orientation and nanotube fiber angle indicated. In *VV* and *VH* the first letter corresponds to the unchanged incident polarization always at 0°. The second letter corresponds to the analyzer orientation, either parallel (*V*) or perpendicular (*H*) to the incident polarization. The first column (top) indicates the fiber angle relative to the incident polarization during the measurement. The various ratios formed from the intensities are given in the columns below and to the right of the data. For example, the last entry appearing in the *VV* set of ratios under 1592 cm^{-1} (value 2.5) is the ratio formed between the 1592 cm^{-1} peak intensities measured in the *VV* geometry at 45° and 90°. The numbers in parentheses next to the ratios are the corresponding calculated ratios.

	VV		*VH*		Ratios	
Angle\Peak	1592 cm^{-1}	202 cm^{-1}	1592 cm^{-1}	202 cm^{-1}	1592*VV*/*VH*	202*VV*/*VH*
0°	47 870	74 490	7 460	9 890	6.4 (7.1)	7.5
23°	36 370	52 430	11 570	13 120	3.1 (4.4)	4.0
45°	24 060	33 010	18 820	20 530	1.3 (2.2)	1.6
90°	9 750	15 580	6 180	7 750	1.6 (1.5)	2.0

Ratios:	$VV_{\theta 1}/VV_{\theta 2}$		$VH_{\theta 1}/VH_{\theta 2}$	
0°/23°	1.3 (1.2)	1.4	0.6 (0.7)	0.8
0°/45°	2.0 (1.9)	2.3	0.4 (0.6)	0.5
0°/90°	4.9 (4.6)	4.8	1.2 (1.0)	1.3
23°/45°	1.5 (1.6)	1.6	0.6 (0.8)	0.6
23°/90°	3.7 (3.8)	3.4	1.9 (1.3)	1.7
45°/90°	2.5 (2.4)	2.1	3.0 (1.7)	2.6

intensities for the corresponding measurement. We note that the model considers only tubes that are misaligned from the fiber axis in a plane perpendicular to the Poynting vector of the incident excitation. This is justified by the presumed small penetration depth, probing only nanotubes at the surface of the fiber. That is, a nanotube which is canted at an angle away from the laser propagation direction contributes to the misaligned tube intensity for only the excitation penetration depth (presumably short under the resonance conditions here).

Table I lists the peak intensities of the ~1592 and 202 cm^{-1} bands as a function of the polarizer–analyzer and fiber orientations. Differences in various orientations between the intensities of the 1592 cm^{-1} and the 1560 and 1545 cm^{-1} are so small that it is adequate to consider only the 1592 cm^{-1} band. Also shown in Table I are the ratios formed from these intensities. The numbers in parenthesis are the corresponding ratios calculated as described above using the best least-squares fit of $p=0.86$ and $\theta=31°$, respectively. The agreement is seen to be quite good. The fit parameters, which arrive at 86% of the nanotubes lying within ±31° of the fiber axis also correlate well with the TEM and SAED results. The larger discrepancy appearing in the *VH*45/*VH*90 measurement could signal some contribution from a form of the second term in Eq. (2) above, unaccounted for in our model. Alternatively, we note that the model also does not account for additional Raman signal from scattered Rayleigh light. This would be largest for this particular ratio since scattered Rayleigh light rotated to the 45° angle of the fiber in the *VH*45 measurement, could now induced Raman scattering at 45°, a component of which would now pass through the cross-polarized analyzer.

Raman scattering measurements on disordered SWNTs drop dried on Si give a depolarization ratio (*VH*/*VV*) of 0.36. Applying our model to this case by integrating over all angles (parallel to the surface), we calculate the depolarization ratio 0.33. Thomsen *et al.*,[13] based on their measured depolarization ratio of 0.40±0.04 for Raman spectra of disordered SWNTs, concluded that the high-energy modes at about 1590 and 1560 cm^{-1} are incompatible with E_g modes (for which the depolarization ratio should be 0.75). They suggest that the absence of E_g modes occurs because of cancellations in the "Raman polarizability" of the traceless eigenmodes. This assumes that the term of the second form in Eq. (2) above dominates the scattering. Based on our results, which indicate that the orientation dependence of $d\underline{\alpha}/dq$ is the same as that of $\underline{\alpha}$ itself, we conclude rather, that the form of the first term dominates. This is *not* to say, however, that the observed Raman lines necessarily contain appreciable intensity from E_g modes. In the first term of Eq. (2) the intensity in each mode is governed by the magnitude of $d\omega_o/dq$. It stands to reason that this will, in fact, be largest for a symmetric mode in which the greatest number of bonds are simultaneously distorted in the same direction (as opposed to an asymmetric mode in which bonds are simultaneously distorted in opposing directions). Detailed, orientation-dependent, *resonance* Raman intensity calculations are clearly called for.

Recently, a study of polarized Raman spectroscopy of aligned multiwalled carbon nanotubes (MWNTs) has appeared.[14] This shows satisfactory agreement with the theory of Ref. 8. In particular, for the *VV* geometry, as the aligned MWNT fiber is tilted from 0° to 90° with respect to the polarization axis, the tangential modes near 1600 cm^{-1} display an intensity minimum at 55°. As shown in Fig. 3, in contrast to the result for the aligned MWNT, the Raman intensity of these modes for the aligned SWNT fiber decreases monotonically in going from 0° to 90°, with no minimum at 55°. This difference between the MWNT and SWNT is probably due to a progressive decrease in the importance of the first term of Eq. (2), with increasing nanotube diameter (see, e.g., Ref. 7).

V. CONCLUSION

To summarize, we have:

1. Described a simple method for producing (neat) fibers of nanotubes in which the tubes display substantial alignment along the fiber axis.

2. Measured the polarization-dependent Raman scattering of these aligned nanotube fibers as a function of fiber angle.

3. Shown qualitatively how, contrary to normal Raman scattering, this can result in a nanotube Raman intensity having the same orientation dependence as the polarizability of the nanotube.

4. Experimentally verified that for laser excitation energies about 1.92 eV, interband transitions are only available for the polarization component parallel to the nanotube axis.

5. Within a model accounting for the misaligned nanotubes making up our fibers, demonstrated reasonable agreement with the idea summarized in 3.

ACKNOWLEDGMENTS

The authors thank David Tanner, Chris Stanton, and Selma Hershfield for helpful discussions. This work was supported in part by U.S. Navy Contract No. N00173-99-C-2000.

[1] J. W. G. Wildoer, L. C. Venma, A. G. Rinzler, R. E. Smalley, and C. Dekker, Nature (London) **391**, 59 (1998).
[2] T. W. Odom, J. L. Huang, P. Kim, and C. M. Lieber, Nature (London) **391**, 62 (1998).
[3] A. Thess, R. Lee, P. Nikolaev, H. Dai, P. Petit, J. Robert, C. Xu, Y. H. Lee, S. G. Kim, A. G. Rinzler, D. T. Colbert, G. E. Scuseria, D. Tomanek, J. E. Fischer, and R. E. Smalley, Science **273**, 483 (1996).
[4] C. Journet, W. K. Maser, P. Bernier, A. Loiseau, M. L. Delachapelle, S. Lefrant, P. Deniard, R. S. Lee, and J. E. Fischer, Nature (London) **388**, 756 (1997).
[5] A. M. Rao, E. Richter, S. Bandow, B. Chase, P. C. Eklund, K. A. Williams, S. Fang, K. R. Subbaswamy, M. Menon, A. Thess, R. E. Smalley, G. Dresselhaus, and M. S. Dressehaus, Science **275**, 187 (1997).
[6] E. Richter and K. R. Subbaswamy, Phys. Rev. Lett. **79**, 2738 (1997).
[7] A. G. Rinzler, J. Liu, H. Dai, P. Nikolaev, C. B. Huffman, A. H. Lu, D. Heymann, D. T. Colbert, R. S. Lee, J. E. Fischer, A. M. Rao, P. C. Eklund, and R. E. Smalley, Appl. Phys. A: Mater. Sci. Process. **67**, 29 (1998).
[8] R. Saito, T. Takeya, T. Kimura, G. Dresselhaus, and M. S. Dresselhaus, Phys. Rev. B **57**, 4145 (1998).
[9] H. Ajiki and T. Ando, Physica B **201**, 349 (1994).
[10] J. Hwang, H. H. Gommans, A. Ugawa, D. B. Tanner, and A. G. Rinzler (unpublished).
[11] J. D. Jackson, *Classical Electrodynamics*, 2nd ed. (Wiley, New York, 1975).
[12] M. Cardona, *Resonance Phenomena in Light Scattering from Solids II* (Springer, Berlin, 1982).
[13] C. Thompsen, S. Reich, P. M. Rafilov, and H. Jantoljak, Phys. Status Solidi B **214**, R15 (1999).
[14] A. M. Rao, J. Jorio, M. A. Pimenta, M. S. S. Dantas, G. Dresselhaus, and M. S. Dresselhaus, Phys. Rev. Lett. **84**, 1820 (2000).